



6-27-2022

## Experimental Radial Profiles of Early Time (<math><4 \mu\text{s}></math>) Neutral and Ion Spectroscopic Signatures in Lightning-Like Discharges

M. Passas-Varo

*Instituto de Astrofísica de Andalucía (IAA), Granada, Spain*

F. J. Gordillo-Vazquez

*Instituto de Astrofísica de Andalucía (IAA), Granada, Spain*

J. Sanchez

*Instituto de Astrofísica de Andalucía (IAA), Granada, Spain*

Ny Kieu PhD

*Loyola University Chicago, nkieu@luc.com*

Follow this and additional works at: [https://ecommons.luc.edu/physics\\_facpubs](https://ecommons.luc.edu/physics_facpubs)



Part of the [Physics Commons](#)

### Recommended Citation

Passas-Varo, M.; Gordillo-Vazquez, F. J.; Sanchez, J.; and Kieu, Ny PhD, "Experimental Radial Profiles of Early Time (<math><4 \mu\text{s}></math>) Neutral and Ion Spectroscopic Signatures in Lightning-Like Discharges" (2022).

*Physics: Faculty Publications and Other Works*. 68.

[https://ecommons.luc.edu/physics\\_facpubs/68](https://ecommons.luc.edu/physics_facpubs/68)


This Article is brought to you for free and open access by the Faculty Publications and Other Works by Department at Loyola eCommons. It has been accepted for inclusion in Physics: Faculty Publications and Other Works by an authorized administrator of Loyola eCommons. For more information, please contact [ecommons@luc.edu](mailto:ecommons@luc.edu).



This work is licensed under a [Creative Commons Attribution-No Derivative Works 4.0 International License](#).

© 2022. The Authors.

## Experimental Radial Profiles of Early Time ( $<4 \mu\text{s}$ ) Neutral and Ion Spectroscopic Signatures in Lightning-Like Discharges

M. Passas-Varo<sup>1</sup> , F. J. Gordillo-Vázquez<sup>1</sup>, J. Sánchez<sup>1</sup>, and N. Kieu<sup>2</sup>

<sup>1</sup>Instituto de Astrofísica de Andalucía (IAA), CSIC, Glorieta de la Astronomía s/n, Granada, Spain, <sup>2</sup>Physics Department, Loyola University, Chicago, IL, USA

### Key Points:

- Dynamics of radial spectroscopic structure (up to 16 mm) of heated lightning-like channels is explored. Gas temperature peaks at the edge
- Early (0.72  $\mu\text{s}$ ) radial optical emissions are due to molecules. Ions and atom emissions dominate at later times ( $\geq 1.83 \mu\text{s}$ )
- OH is found to be the second most abundant molecular species (after nitrogen oxide) directly generated by heated lightning-like channels

### Correspondence to:

M. Passas-Varo,  
passasv@iaa.es

### Citation:

Passas-Varo, M., Gordillo-Vázquez, F. J., Sánchez, J., & Kieu, N. (2022). Experimental radial profiles of early time ( $<4 \mu\text{s}$ ) neutral and ion spectroscopic signatures in lightning-like discharges. *Journal of Geophysical Research: Atmospheres*, 127, e2022JD036553. <https://doi.org/10.1029/2022JD036553>

Received 24 JAN 2022  
Accepted 13 JUN 2022

### Author Contributions:

**Conceptualization:** M. Passas-Varo, F. J. Gordillo-Vázquez, J. Sánchez  
**Data curation:** M. Passas-Varo  
**Formal analysis:** M. Passas-Varo, F. J. Gordillo-Vázquez  
**Funding acquisition:** F. J. Gordillo-Vázquez  
**Investigation:** M. Passas-Varo, F. J. Gordillo-Vázquez, J. Sánchez  
**Methodology:** M. Passas-Varo, F. J. Gordillo-Vázquez, J. Sánchez  
**Project Administration:** F. J. Gordillo-Vázquez  
**Resources:** F. J. Gordillo-Vázquez, J. Sánchez  
**Software:** M. Passas-Varo

© 2022. The Authors.

This is an open access article under the terms of the [Creative Commons Attribution-NonCommercial-NoDerivs License](https://creativecommons.org/licenses/by/4.0/), which permits use and distribution in any medium, provided the original work is properly cited, the use is non-commercial and no modifications or adaptations are made.

**Abstract** This study presents experimental results for the radial and temporal variation of neutral and ion spectroscopic signatures emerging from the heated channel of lightning-like discharges diagnosed with a high speed (900,000 fps) imaging spectrograph. Light emissions emanate from three regions: an inner core (up to  $\sim 2$  mm), an external sheath (up to  $\sim 4$  mm) featuring a sudden temperature increase, and further optical emissions forming a dim glow from 4 mm up to 16 mm. The optical emissions are initially ( $<1.11 \mu\text{s}$ ) dominated by the  $\text{N}_2$  first positive system at 660.8 nm and by the N II ion line at 661.05 nm. Between 1.11 and 3.33  $\mu\text{s}$  the optical emissions are dominated by  $\text{H}_\alpha$  (656.3 nm) and O II ion (656.54 nm) lines. The N II ion line at 648.20 nm prevails in the outer dim glow region (9–12 mm) before 2.22  $\mu\text{s}$ . Spectroscopic signals were used to experimentally derive the time dynamics of the electron density and electron/gas temperature radial profiles, which allowed the estimation of the early time overpressure pulse, electrical conductivity and concentrations of key molecular species ( $\text{N}_2$ , NO,  $\text{O}_2$ , OH,  $\text{H}_2$ ,  $\text{N}_2\text{O}$ ,  $\text{NO}_2$ ,  $\text{HO}_2$ ,  $\text{O}_3$ , and  $\text{H}_2\text{O}$ ) along the radial axis of the heated air plasma channel. These populations were calculated from the overpressure pulse, assuming that they were produced from humid (50%) air under thermal equilibrium conditions. OH is found to be the second most abundant molecular species (after NO) directly generated by heated lightning-like channels.

**Plain Language Summary** The present work explores the temporal evolution (with submicrosecond time resolution) of spectroscopic optical emissions along the radial dimension of lightning-like channels. Such study can contribute to quantify the radial variation of the gas temperature and electron density, and to explore their influence on the direct early production of important neutral (atoms and molecules) and ion species along the heated channel. Our study has found that the gas temperature peaks at the edge of the channel and that early (0.72  $\mu\text{s}$ ) radial optical emissions are dominated by molecules followed by ions and atoms that also prevail at later times. The study also suggests that hydroxyl (OH) could be the second most abundant molecular species (after nitrogen oxide) directly generated by heated lightning-like channels.

## 1. Introduction

Slitless spectroscopy is a well known technique to analyze the absorption and emission of light coming from a narrow source, that consists of an optical system including a diffraction element and a sensor. It is a very useful tool to analyze the spectrum of natural (Boggs et al., 2021; Orville, 1968; Prueitt, 1963; Uman, 1963) and triggered lightning (Walker & Christian, 2019; Weidman et al., 1989) since it provides a wide field of view which usually allows to capture the whole lightning stroke in the camera sensor, which not only permits to measure the electron density and temperature in the lightning core (Prueitt, 1963; Uman, 1963; Walker & Christian, 2017, 2019), but also vertical temperature profiles in natural lightning return strokes (Boggs et al., 2021). Unfortunately, slitless spectroscopy makes difficult to discern wavelengths among nearly coincident lightning flashes, besides the serious limitations it presents for wavelength and, especially, for flux calibrations that could negatively affect spectral data reduction. Moreover, to date, slitless spectroscopy studies do not provide a direct measurement of the radial features of the lightning stroke channel, due to the low spatial resolution of the instruments in the radial dimension. Despite this inconvenience, recent studies have theoretically estimated the radial profile of the lightning channel temperature from the direct quantification of the gas temperature in the core of the lightning channel through the solution of the heat transfer differential equation (An et al., 2019; Bocharov et al., 2021; Ripoll, Zinn, Colestock, & Jeffery, 2014; Ripoll, Zinn, Jeffery, & Colestock, 2014; Sousa-Martins et al., 2016, 2019).

On the other hand, slit spectroscopy includes a very narrow slit in the optical path so it is possible to analyze a narrow area from wider light sources, becoming an ideal tool for the optical diagnosis of distant plasmas

**Supervision:** M. Passas-Varo, F. J. Gordillo-Vázquez  
**Validation:** M. Passas-Varo, F. J. Gordillo-Vázquez, J. Sánchez  
**Visualization:** M. Passas-Varo, J. Sánchez, N. Kieu  
**Writing – original draft:** M. Passas-Varo  
**Writing – review & editing:** F. J. Gordillo-Vázquez

such as transient luminous events (Gordillo-Vázquez et al., 2018), emissions from meteor luminous trails (Passas, Madiedo, et al., 2016; Passas, Sánchez, et al., 2016), natural lightning (Dufay, 1926; Slipher, 1917) or lightning-like plasma channels (Kieu et al., 2020, 2021). This technique results especially useful to analyze laboratory plasmas, since we can predict the plasma channel location and, therefore, we can aim the system so the plasma channel can be easily imaged on the slit. It provides a higher radial and spectral resolution compared with slitless spectroscopy, and allows a direct measurement of the radial profiles of electron density and temperature in the plasma channel. Moreover, the wavelength and flux calibration of slit spectrographs are trustful and easy to develop and reproduce (Fantz, 2006; Parra-Rojas et al., 2013; Passas, Madiedo, et al., 2016; Passas, Sánchez, et al., 2016; Passas-Varo et al., 2019).

The analysis of the spectrum of distant plasmas allows to infer physical properties as the gas temperature or the electron density. So far, the method to obtain a spectral curve from 2D spatial-spectral images, consists of integrating the entire image in the spatial dimension, so the signal-to-noise ratio (SNR) is enhanced in the spectral dimension (Kieu et al., 2020, 2021). However, this method usually ignores the spatial information that could reveal the radial distribution of electron density and/or temperature from the core of the lightning-like plasmas to its surface.

In this paper we focus on the radially resolved slit spectroscopy of 20 laboratory-produced lightning-like discharges in air of ~30 mm length using the GrAnada Lightning Ultrafast Spectrograph (GALIUS) (Passas-Varo et al., 2019) in the visible (645.0–663.0 nm) region operated at 900 kfps with 0.79  $\mu$ s exposure time and spectral resolution better than 0.38 nm. This allows us to experimentally quantify the profiles of electron density and temperature along the radial dimension of the lightning-like plasma channels and their temporal dynamics. From these measurements we also estimate the evolution of the radial profiles of the electrical conductivity and overpressure. Furthermore, by using the overpressure peak profile, we estimate the populations of important molecular species ( $N_2$ , NO,  $O_2$ , OH,  $H_2$ ,  $N_2O$ ,  $NO_2$ ,  $HO_2$ ,  $O_3$ , and  $H_2O$ ) produced along the radius of the plasma channel, assuming that they were produced from humid (50%) air under thermal equilibrium conditions.

## 2. Instrumentation and Experimental Setup

Figure 1 shows a schematic of the experimental setup we used. It consists of the above-mentioned GALIUS ultrafast imaging spectrograph, a photometer, a field camera and an electrostatic generator, both first being placed on an optical rail that allows a correct alignment.

GALIUS is a portable, ground-based slit spectrograph able to record spectra of natural/triggered lightning or lightning-like plasmas with submicrosecond time resolution thanks to a very high sensitivity Photron SA-Z camera. GALIUS can be set up with a total of 22 configurations made of combinations of 10 collector lenses, 2 collimator lenses in the near UV and visible-NIR range and 4 high spectral resolution interchangeable volume-phase holographic (VPH) gratings (Arns et al., 1999; Hill et al., 2003).

For the results presented here, GALIUS was set up in slit mode (50  $\mu$ m  $\times$  3 mm) with a collimator lens of 50 mm (F#11) combined with a collector lens of 60 mm (F#1.5) focal length, and a grism of 1,855 lines/mm with its central wavelength at  $\approx$ 654 nm providing a spectral resolution better than 0.38 nm. We set up a recording speed of 900 kfps combined with a exposure time of 0.79  $\mu$ s, that allowed a maximum sensor area of 56  $\times$  128 pixels, providing a spectral bandwidth of 18 nm due to the spectral dispersion of GALIUS under this setup. We chose the spectral range to be between 645 and 663 nm to simultaneously measure the N II ion lines at 648.20 and 661.05 nm, and the H I neutral line at 656.27 nm, which allowed us to calculate the radial profile and its variation with time of the electron (gas) temperature and the electron density of the plasma channel, following the methods explained in next section. Full description of GALIUS can be found in Passas-Varo et al. (2019). Table 1 summarizes GALIUS setting parameters. The distance between every spark and the collector lens was 680 mm  $\pm$  5 mm.

The photometer synchronizes the GALIUS Photron SA-Z camera with the initial stage of a luminous event. This is done with a TTL trigger to avoid collapsing the internal buffer of GALIUS camera with empty images. It works with a typical delay of 220 ns.

Voltage and current from the spark are measured by a TESTEC TT HVP 15HF high voltage probe and a Chauvin Arnoux Miniflex MA200 insulated flexible AC current probe, respectively. Both probes are connected to a RS PRO IDS-1104B oscilloscope, that also measures the photometer response through a BNC connector. The delay

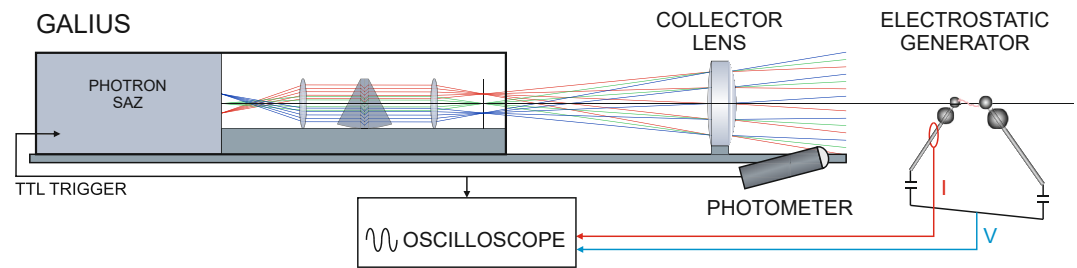


**Figure 1.** Experimental setup that consists of the GrAnada Lightning Ultrafast Spectrograph (GALIUS) ultrafast imaging spectrograph, a photometer and an electrostatic generator, both first being placed on an optical rail that allows a correct alignment. The RS PRO IDS-1104B oscilloscope measures the photometer response, the voltage and the current from the spark.

of the camera trigger is calculated from the mean time between the instant at half rising up of the photometer response and the instant at half rising up of the current between electrodes.

The electrostatic generator is an automated Wimshurst machine of dimensions  $360 \times 250 \times 400 \text{ mm}^3$  and contra-rotating discs of 310 mm diameter, that generates lightning-like plasmas (sparks) of variable length, depending on the distance between electrodes. The path between electrodes is placed perpendicular to the optical rail so the spark plasma-channel is horizontal and also perpendicular to the optical rail. Figure 2 shows the area of the plasma channel that projects on the slit.

The field camera is provided with a sensor of  $1,280 \times 720$  pixels and a frame rate of 30 fps that records a video of every discharge. A spatial pattern between electrodes is also recorded to estimate the spatial dimensions of every spark.

### 3. Methodology

In this study we have analyzed the electric features, field images and 2D spatial-spectral images of 20 lightning-like plasmas and their evolution in time.

We estimated the injected energy in the 30 mm sparks from the oscilloscope electric signals of current and voltage; from the field images we characterized the dimensions of the lightning-like plasmas thanks to a calibrated pattern we placed between electrodes. Besides, the 2D spatial-spectral images allowed us to experimentally derive the radial profiles of electron/gas temperature, electron density, and from them to deduce the electrical conductivity and overpressure in the air plasma discharge. Moreover, the concentrations of key molecular species ( $\text{N}_2$ , NO,  $\text{O}_2$ , OH,  $\text{H}_2$ ,  $\text{N}_2\text{O}$ ,  $\text{NO}_2$ ,  $\text{HO}_2$ ,  $\text{O}_3$ , and  $\text{H}_2\text{O}$ ) along the radial axis of the heated air plasma channel were calculated from the overpressure pulse, assuming that they were produced from humid (50%) air under thermal equilibrium conditions.

The typical time scale of our lightning-like discharge is much shorter than that of a real and/or triggered lightning air plasma because, in real lightning, the injected current can last for tens to hundreds of microseconds. However, this does not invalidate our results. We see a number of spectral (and derived magnitudes) similarities between our discharge (that we call lightning-like discharge) and a real and/or triggered lightning plasma: (a) ionic lines dominate over neutral lines ( $\text{H}_\alpha$  at 656.2 nm) in the early (sub-microsecond) temporal stage (see also Figures 1e and 1f in Kieu et al. (2020), where the same lightning-like discharge was used), (b) at later times (beyond 1  $\mu\text{s}$ ), the intensities of atomic lines ( $\text{H}_\alpha$  at 656.2 nm) are much more intense than those of ionic lines, and (c) both temperature and electron density in our

**Table 1**  
GALIUS Setting Parameters

Collector lens	60 mm F#1.5
Slit dimensions	$50 \mu\text{m} \times 3 \text{ mm}$
Collimator lens	50 mm F#8
Grism	1,855 lines/mm
Camera lens	50 mm F#8
Sensor area	$56 \times 128$ pixels
Recording speed	900 kfps
Exposure time	0.79 $\mu\text{s}$
Central wavelength	656.2 nm
Spectral range	645–663 nm
Spectral dispersion	0.14 nm/px
Spatial dispersion	0.58 mm/px
Spectral resolution	$\leq 0.38 \text{ nm}$

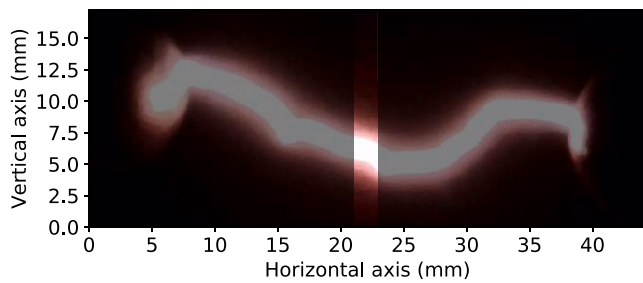


**Figure 2.** Spark number 7. The non-shadowed area is the region of the spark projected on the GrAnada Lightning Ultrafast Spectrograph (GALIUS) vertical slit.

discharge are similar to those obtained in natural lightning (Orville, 1968) and/or in triggered lightning (Walker & Christian, 2019).

However, spectra of non lightning-like plasmas in air like, for instance, laser-induced air plasmas (that also exhibit shorter times scales than the ones in lightning air plasmas), show intensities of atomic lines that are similar to those of ionic lines at times beyond 1  $\mu$ s (Cen et al., 2022). Another interesting feature is that in regular (non lightning-like) air plasmas at any time scale (early or late), the  $H_{\alpha}$  line is much weaker than in the spectrum of lightning and/or lightning-like plasmas. This is well illustrated in the recent paper by Cen et al. (2022) where time resolved spectra of a real natural lightning is compared with time resolved spectra of a laser-produced plasma in air. Finally, early time temperatures in laser-produced plasmas in air are half of those in lightning and/or lightning-like air plasmas, and early time electron densities in laser-produced air plasmas are a factor of two lower than in lightning and/or lightning-like air plasmas.

All the above support our approach of using a type of electric (spark) discharge in air that shares many similarities with real lightning and/or triggered lightning. Other types of air thermal plasmas should not be properly considered lightning-like discharges in air.

### 3.1. Time Resolved Spectra and Radial Profile of Brightness

Figure 2 shows a horizontal lightning-like discharge (spark) while the GALIUS slit is placed vertically. Hence, the 2D spatial-spectral images of the spark are the projection of the spectrum of a plasma slice on the CMOS sensor, with the vertical dimension including the spatial information, whereas the horizontal dimension corresponds to the spectral information. In other words, every column of pixels of the spatial-spectral image corresponds to a different wavelength, and every row of pixels of the spatial-spectral image corresponds to a different radial position of the investigated sparks.

After recording the raw spatial-spectral images, we reduced them as previously described in Kieu et al. (2020) and Passas-Varo et al. (2019).

By analyzing the reduced spatial-spectral images row by row, we can estimate several physical parameters of the lightning-like discharges, such as the gas temperature and the electron density in every radial position of the region of the plasma discharge that is projected on the slit. To do so, we only consider those rows with an acceptable SNR, that is, we only accept the rows that show values of intensity at 648.20 nm (N II ion line), 656.27 nm (H I neutral line also known as  $H_{\alpha}$ ) and 661.05 nm (N II ion line) higher than three times the standard deviation of the signal for that row. These are the lines used to quantify the electron density ( $H_{\alpha}$ ) and the electron/gas temperature (N II ions at 648.20 and 661.05 nm).

On the other hand, if we integrate the values of all columns of the reduced spatial-spectral images, we obtain the radial profiles of the brightness of the region of plasma discharges that are projected on the slit, and their evolution with time.

### 3.2. Electron/Gas Temperature

We calculated the radial profile and its variation with time of the electron/gas temperature of every lightning-like plasma by following the procedure described in Prueitt (1963) and Uman (1963) for every row of the 2D reduced spatial-spectral image, considering that (a) the channel of the lightning-like discharge is optically thin (there is no light absorption through the line of sight), (b) the temperature is relatively uniform along the lightning-like channel radial cross section (temperatures are similar at the edge and the center of the lightning channel), and (c) that thermal equilibrium controls the concentration of the different atoms, molecules and ion energy levels emitting light due to spontaneous radiative deexcitation, that is, the density of excited atoms, molecules and ions follow Boltzmann's law. We also assume that local thermal equilibrium (LTE) applies so that the derived electron temperature equals the gas temperature. Note that in LTE all quantities depend only on the gas temperature.

Equation 1 is found in Walker and Christian (2019) and it is used to calculate the electron/gas temperature of the lightning channel, from the ratio of the areas below N II ion lines at 648.20 nm ( $I_{nr}$ ) and 661.05 nm ( $I_{mp}$ ) of each row of the 2D reduced spatial-spectral image. We only take into account those rows which values of intensity of the N II ion lines that are three times higher than the standard deviation of the signal for that row (values over 3-sigma) (Thomsen et al., 2003). This ensures that we have real values of temperature instead of mathematical artifacts. Notice that  $k$  is the Boltzmann constant and  $E_{m,n}$ ,  $A_{m,n}$ ,  $g_{m,n}$ , and  $\nu_{m,n}$  are well-known constants associated to the upper energies ( $E_{m,n}$ ) of excited electronic levels  $m$  and  $n$  of atoms, molecules and ions that can be found in tables from the National Institute of Standards and Technology (NIST) atomic spectra databases (Kramida et al., 2020).

$$T_e = \frac{E_m - E_n}{kLn \left[ \frac{I_{nr} A_{mp} \nu_{mp} g_m}{I_{mp} A_{nr} \nu_{nr} g_n} \right]} \quad (1)$$

### 3.3. Electron Density

We obtained the variation in time of the electron density radial profile of every spark by following the method described by Gigosos et al. (2003), which analyses the full width at half area (FWHA) of the H I neutral line at 656.27 nm, the so-called  $H_\alpha$  spectral line, for every row of the reduced 2D spatial-spectral images, and connects it with the electron density through Equation 2. This method is independent of any assumptions on the equilibrium state of the air plasma.

$$N_e = 10^{17} \left( \frac{FWHA}{1.098} \right)^{1.47135} \text{ cm}^{-3}. \quad (2)$$

First, we isolated the  $H_\alpha$  broadened spectral line from other emissions. To do so, we fitted every row spectrum with the sum of three Lorentzian curves, each of them centered in the wavelengths of the strongest spectral lines of the observed spectra: 648.20 nm (N II), 656.27 nm ( $H_\alpha$ ), and 661.05 nm (N II). Then we calculated the FWHA of the Lorentzian curve obtained from the  $H_\alpha$  fitting parameters. We only took into account those rows where the peak value of  $H_\alpha$  was three times higher than the standard deviation of the signal for that row (values over 3-sigma) to ensure that we had real values of electron density instead of noise (Kieu et al., 2021).

### 3.4. Electrical Conductivity

We calculated the radial profile and its variation with time of the electrical conductivity of every spark using the electron density and temperature radial profiles obtained before using the equations in Raizer and Allen (1991). To do so, we assume isotropic collisions so that the momentum transfer cross section  $\sigma_{tr} = \sigma_c$ , with  $\sigma_c$  being the cross section for electron-neutral collisions. As the heated channel is highly ionized ( $N_e/N \geq 10^{-3}$ ), we also assume that the ion ( $N_i$ ) and electron ( $N_e$ ) densities are similar so the effective collision frequency for momentum transfer  $\nu_m = N\nu\sigma_{tr} + N_e\nu\sigma_{Coulomb} \simeq N_e\nu\sigma_{Coulomb}$ , where  $N$  is the gas density,  $\nu$  is the mean thermal velocity of electrons, and  $\sigma_{Coulomb}$  is the cross section of electron-ion collisions dominated by Coulomb forces. We can consider that the electrical conductivity  $\sigma$  in the heated lightning-like channel is controlled by  $\sigma_{Coulomb}$  as (Raizer & Allen, 1991):

$$\sigma_{Coulomb} = \frac{e^2 N_e}{m\nu_m} = 1.9 \times 10^4 T_e (eV)^{1.5} \times \ln(\Lambda)^{-1} (Sm^{-1}), \quad (3)$$

with  $e$  and  $m$  being the electron charge and mass, respectively, and

$$\ln(\Lambda) = 13.57 + 1.5 \log(T_e (eV)) - 0.5 \log(N_e (cm^{-3})). \quad (4)$$

### 3.5. Overpressure

We obtained the variation in time of the radial profile of the overpressure in the heated plasma channel with respect to ambient pressure ( $\delta_p = 1$ ) by following the method described in Kieu et al. (2021). For this we use the electron density and temperature radial profiles obtained, and compute the overpressure as

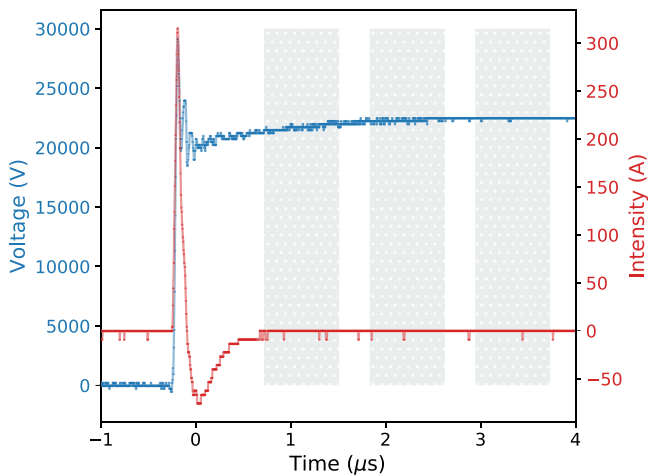


**Figure 3.** Voltage (blue) and current (red) used to generate spark number 7. Dotted gray areas correspond to the exposure time (0.79  $\mu$ s) of the correlative spectral images.

$$\delta_p = \frac{N_e^{\text{exp}}}{N_e^{\text{LTE}(T_g)}}, \quad (5)$$

where  $N_e^{\text{exp}}$  is the electron density obtained experimentally and  $N_e^{\text{LTE}(T_g)}$  is the electron density obtained when equilibrium is assumed at a certain gas temperature.

### 3.6. Equilibrium Composition in a Thermal Plasma of Humid Air

We quantified the temporal variation of the radial profiles of the populations of key molecular species ( $\text{N}_2$ ,  $\text{NO}$ ,  $\text{O}_2$ ,  $\text{OH}$ ,  $\text{H}_2$ ,  $\text{N}_2\text{O}$ ,  $\text{NO}_2$ ,  $\text{HO}_2$ ,  $\text{O}_3$ , and  $\text{H}_2\text{O}$ ) produced along the radius of a humid (50% relative humidity) and heated air plasma channel. For that we have scaled the composition of atmospheric pressure lightning-like air plasmas (78%  $\text{N}_2$  and 22%  $\text{O}_2$ ) calculated at local thermal equilibrium (Kieu et al., 2020) by the  $\delta_p$  factor (overpressure) obtained for each time and radial position. The equilibrium calculations in the Supporting Information for Kieu et al. (2020) were performed in the temperature range 1,000–35,000 K with a method based upon the mass action law and the chemical base concept (Godin & Trépanier, 2004), assum-

ing a relative humidity (RH) of 50% that corresponds to the ambient RH measured in the laboratory during experiments. The chemical species considered were 14 atomic, 24 diatomic, and 44 polyatomic species including electrons, negative ions and single and double positive ions. Internal partition functions were also calculated for atoms, diatomic and polyatomic molecules as well as for positive and negative ions.

As an example, we obtain the populations of OH as

$$OH(T_g) = \delta_p \times OH^{\text{atm,LTE}}(T_g), \quad (6)$$

where  $OH^{\text{atm,LTE}}$  is the local thermal equilibrium of OH at atmospheric pressure. We estimate the populations of all the mentioned molecular species in the same way.

## 4. Results

In this study we have recorded the electric features and the time-resolved images and spectra of 20 sparks of 30 mm length and  $8 \pm 2$  mm mean width, generated by a Wimshurst machine, in a synchronous way, being their mean peak voltage and current 32.70 kV and 149.58 A, respectively, with an injected mean total energy of  $\sim 0.10$  J/cm, calculated for 0.06  $\mu$ s, which corresponds to the time that the current (intensity) pulse remains over the half of its maximum.

We have chosen spark number 7 as an illustrative sample within the 20 measurements we have recorded. The goal of this work is not the comparison between a rare spark and the rest, but to show a real observation and the median value of a significant sample of sparks. Figure 2 shows the section of spark number 7 projected on the GALIUS vertical slit. Figure 3 shows its voltage and current, with maximum values of 29,134 V and 315.24 A, respectively. This provides an injected total electric energy of  $\sim 0.18$  J/cm.

Figures 4 and 5 show the correlative spatial-spectral images and the correlative reduced spectra of spark number 7, respectively, where we can find six strong spectral lines corresponding to two singly ionized N II lines (648.20 and 661.05 nm), two singly ionized O II lines (648.65 and 656.54 nm), the  $\text{H}_\alpha$  line (656.27 nm) and the First Positive System (FPS) of  $\text{N}_2$  (6, 3) line (660.80 nm). Overlapping them, we also find several weaker spectral lines of N I, O II, N II,  $\text{N}_2$ ,  $\text{O}_2^+$ , Ar II, C I and Cu II. We can explain C I presence since, at typical temperatures (4,000–6,000 K) of air in the edge of the expanding channel of a lightning-like discharge, ground state C ( $^3\text{P}$ ) atoms can be efficiently produced through the reaction  $\text{CO}(X^1\Sigma_g^-, v1) + \text{CO}(X^1\Sigma_g^-, v2) \rightarrow \text{CO}_2 + \text{C}(^3\text{P})$  (Carbone et al., 2020). Cu II presence is due to the contamination from the Wimshurst machine copper brushes.

Figures 6 and 7 show the radial profiles of the brightness of the spectral lines of N II (648.20 nm), O II (648.65 nm),  $\text{H}_\alpha$  (656.27 nm), O II (656.54 nm),  $\text{N}_2$  FPS (6, 3) (660.80 nm), and N II (661.05 nm), at different sampling times,

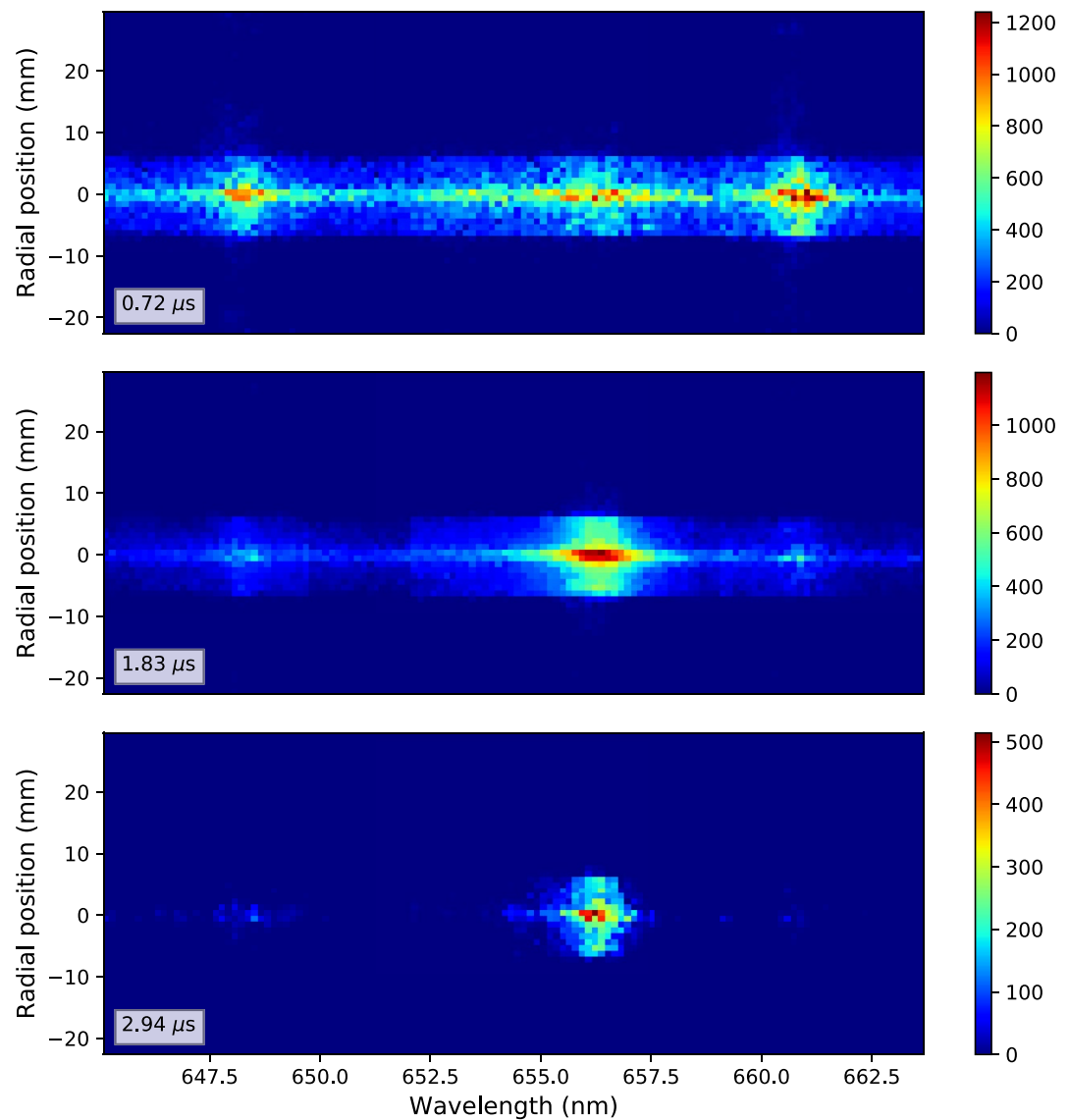


**Figure 4.** 2D correlative spatial-spectral images of spark number 7. The colorbar indicates brightness in arbitrary units (a.u.). Note that in the first two images ( $0.72 \mu\text{s}$ ,  $1.83 \mu\text{s}$ ) the brightness extends beyond  $\sim 7\text{--}8 \text{ mm}$ .

for spark number 7 and for the median value of the 20 recorded sparks respectively. We obtained these radial profiles by plotting the dimensionless brightness of the spectral image at each wavelength, for each radial position. In order to better explain the radial evolution of these ions, atom, and molecule optical emissions we have identified four different regions along the spark radius: an inner core of 2 mm radius that includes regions I and II, wrapped by an outer sheath of up to  $4 \text{ mm} \pm 0.58 \text{ mm}$  radius (region III) and a dim glow region from 4 up to 16 mm (region IV).

When analyzing the radial profile of the spectrum obtained through the median value of the aligned spatial-spectral images of the 20 recorded sparks (Figure 7) we find the same behavior that Figure 6 shows for regions I to III.

The nondimensional radial profile of the brightness of spark number 7 and its evolution in time is shown in all panels of Figure 8 as a purple, blue and greenish transparent shadowed area. We obtained these brightness radial profiles from integrating all the columns of the correspondent spectral image, so the spectral information is lost and the signal-to-noise ratio is maximized in the spatial dimension. Overlapping these radial profiles of brightness, Figure 8 also shows, in black, red and yellow solid lines, the evolution of the radial profile of (a) electron/gas temperature, (b) electron density, (c) electrical conductivity, and (d) overpressure of spark number 7.



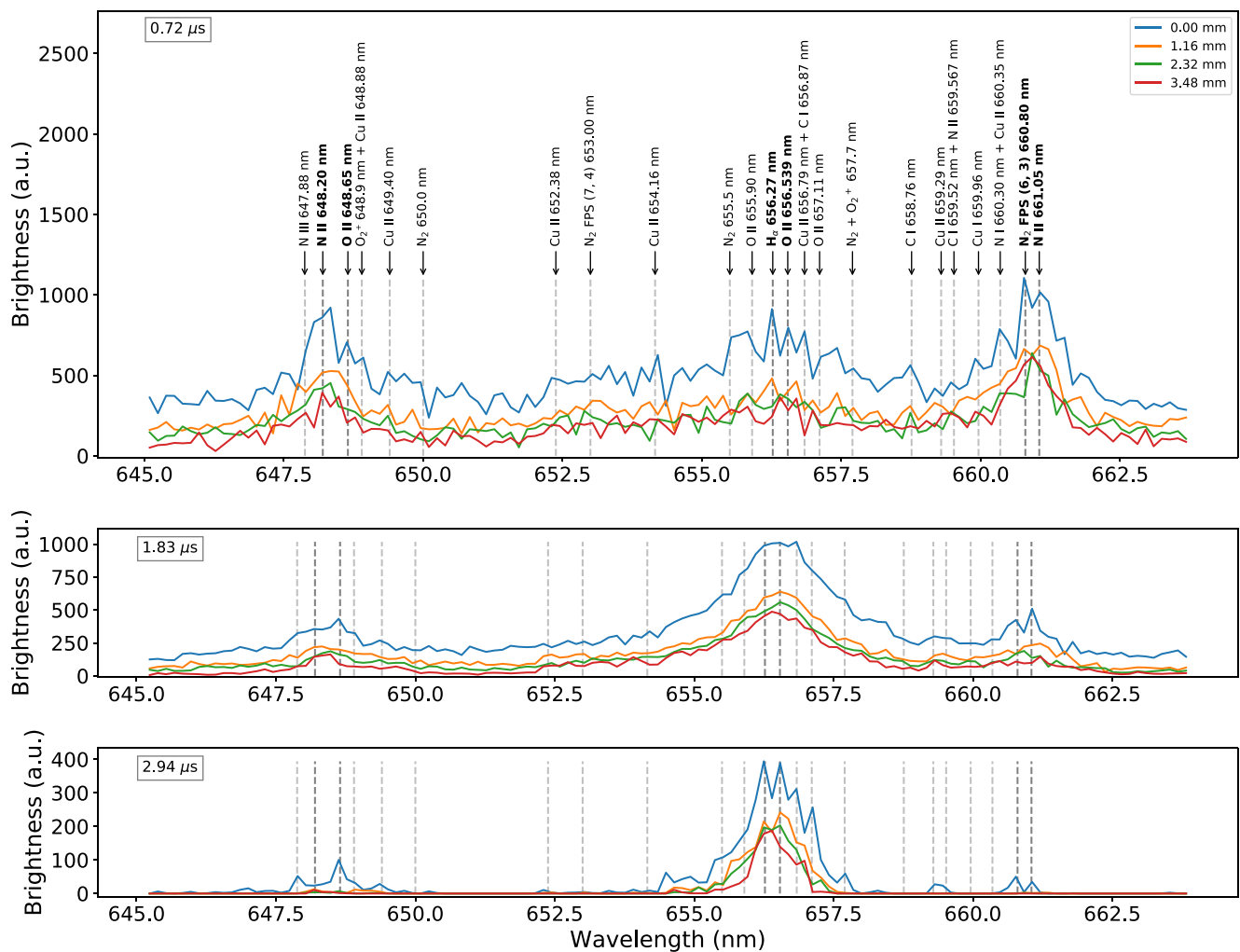


**Figure 5.** Reduced spectra of spark number 7 and its evolution with time at different radial positions (0.00 mm, 1.16 mm, 2.32 mm, 3.48 mm). Strongest emission lines are annotated in the top panel. Radial profiles and temporal evolution of bold emission lines (the six strongest ones) are shown in Figures 6 and 7.

From panel (a) of Figure 8, we notice that the electron temperature of spark number 7 remains almost constant along the inner core of the spark whereas it increases in the external border of the spark sheath. This trend is consistent with the results obtained for times  $\leq 5 \mu\text{s}$  from 1D cylindrical radiation-hydrodynamic simulations using an exact (i.e., the discrete-ordinates method [DOM-S12]) and approximate (i.e., the P1 model approach) solutions of the radiation transfer equation, that are plotted in Figure 4 of Ripoll, Zinn, Jeffery, & Colestock (2014), especially if we compare the radial profile of the temperature of spark number 7 at 2.94  $\mu\text{s}$ , where the electron/gas temperature ranges between 10,000 and 15,000 K. Notice that the modeling considers a lightning of 200 J/cm. Hence, although the shapes of the radial profile of electron/gas temperature are comparable, both the radius and the time scale are far different from the experimental results presented here. This trend is also found in Sousa-Martins et al. (2016, 2019) where the radial profile of the electron temperature of high current pulsed arcs is calculated from experimental data combined with the radiative transfer equation. Bocharov et al. (2021) also predicts this trend through a 2D numerical simulation of high-current pulsed arc discharge in air, and compares it to experimental results that provide the plasma temperature as a function of time and pressure, but not as a function of the radius (Robledo-Martinez et al., 2008).

It is worthwhile to mention that the experiment does not provide valid values of temperature outside the outer sheath of the plasma channel since the SNR of the 2D spatial-spectral image is not high enough in region IV, but one might think that the radial profile of the electron/gas temperature would slowly decrease as we move away from the inner core as the radiative transfer equation (Ripoll, Zinn, Jeffery, & Colestock, 2014; Sousa-Martins

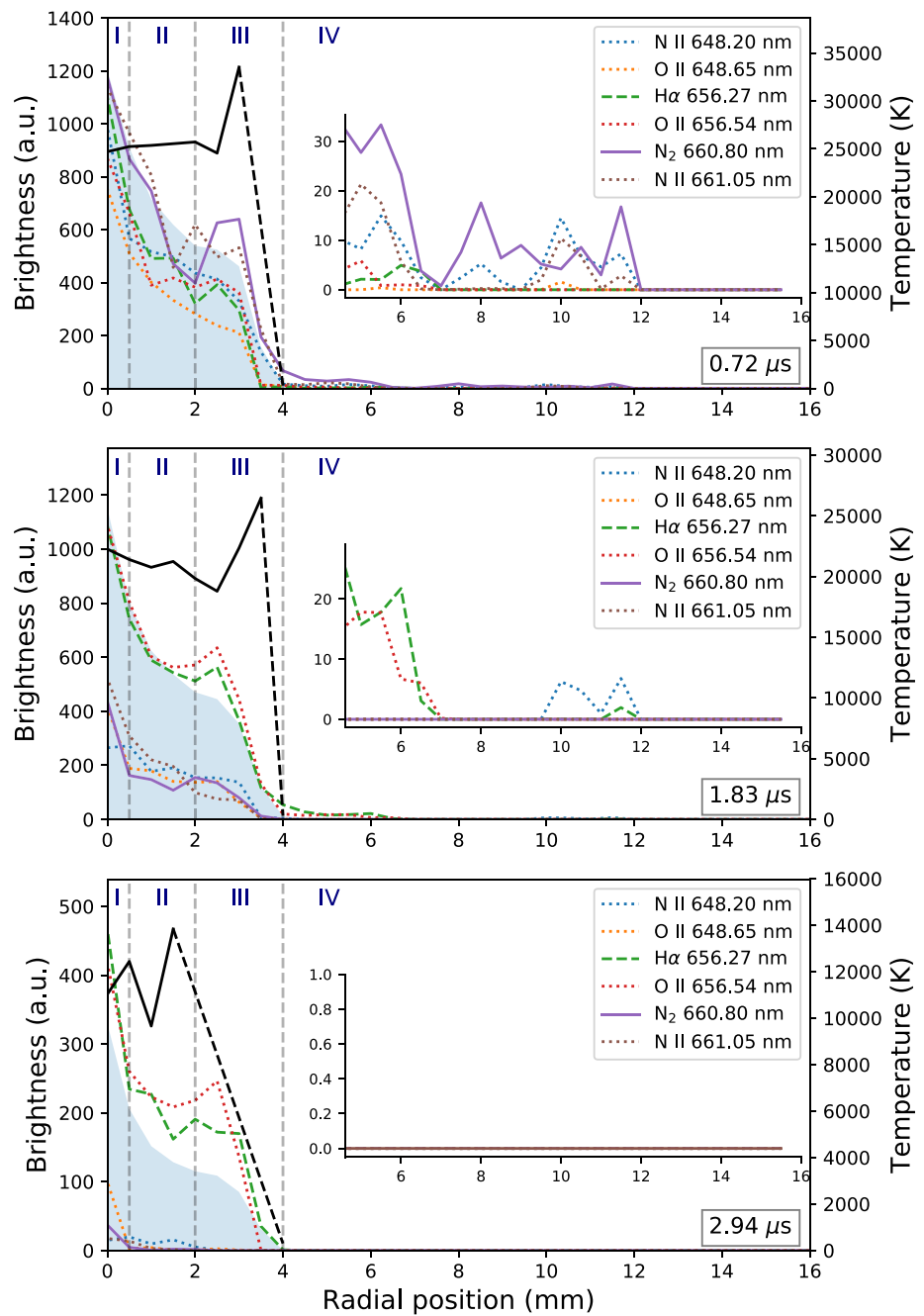


**Figure 6.** Left axes show the radial profile of the brightness (in arbitrary units) of N II (648.20 nm), O II (648.65 nm), H $\alpha$  (656.27 nm), O II (656.54 nm), N $_2$  FPS (6, 3) (660.80 nm), and N II (661.05 nm), at different sampling times, for spark number 7. Right axes show the radial profile of the temperature (black solid lines) and the expected decrease of temperature up to the border of the plasma sheath (black dashed lines). Bluish shape represents the radial profile of the brightness, normalized to the maximum brightness of the spectrum in the core of the spark. Left axes of the inner panels show a zoom in the radial profile of the brightness between 5 and 16 mm. Four different regions are discerned along the spark radius: an inner core of 2 mm radius that includes regions I and II, wrapped by an outer sheath of up to 4 mm  $\pm$  0.58 mm radius (region III) and a dim glow region from 4 up to 16 mm (region IV).

et al., 2016, 2019) suggests. We also found a decrease of the temperature in the inner core as time goes by. As conductivity depends directly on the electron/gas temperature, we also found this same trend in the conductivity radial profile, as panel (c) of Figure 8 shows. This increase of electron/gas temperature and electrical conductivity in the border of the outer sheath of the lightning channel has not been observed neither in previous slit

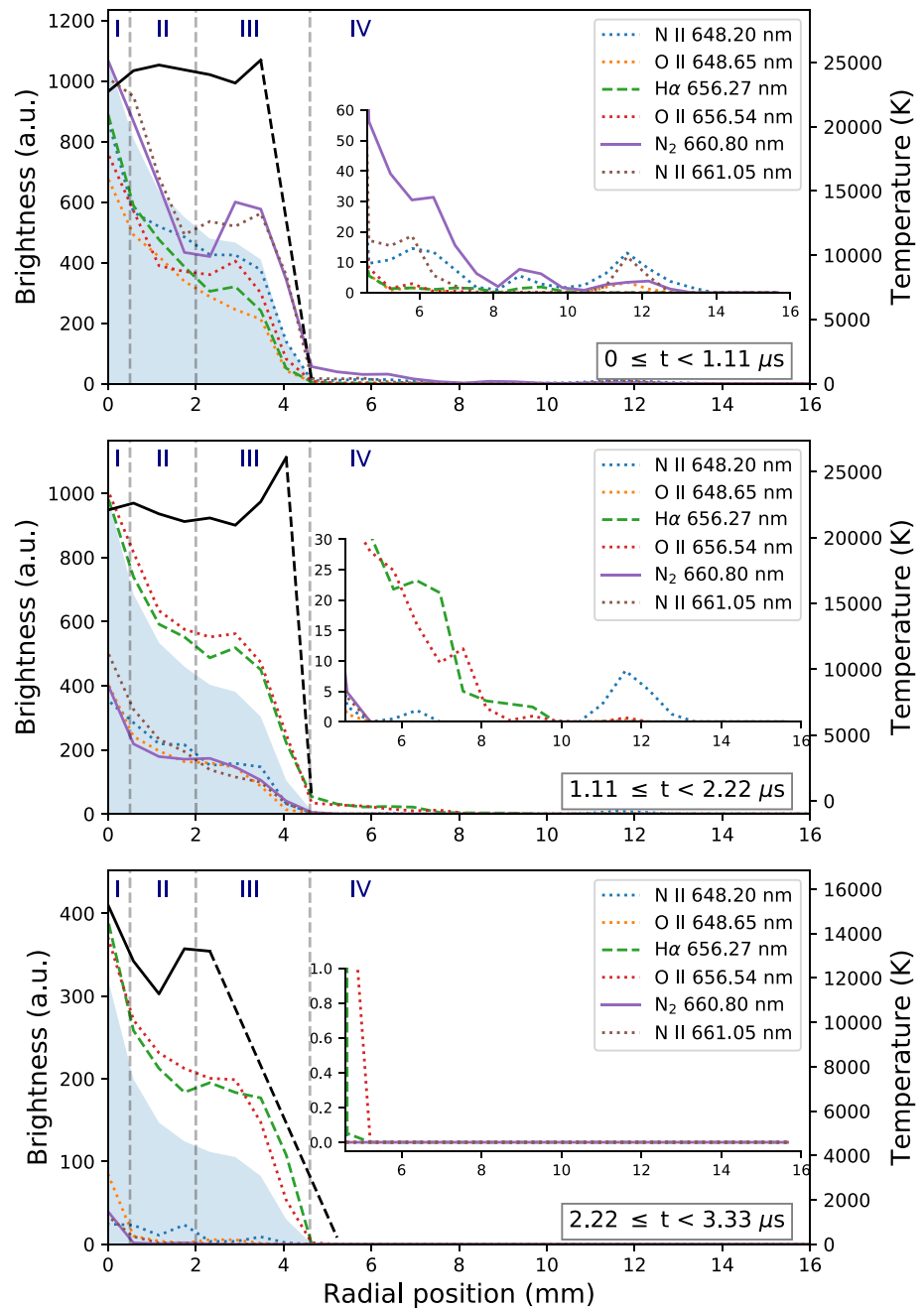


**Figure 7.** Left axes show the radial profile of the brightness (in arbitrary units) of N II (648.20 nm), O II (648.65 nm), H $\alpha$  (656.27 nm), O II (656.54 nm), N $_2$  FPS (6, 3) (660.80 nm), and N II (661.05 nm), at different sampling times, for the median brightness of 20 spark spatial-spectral images. Right axes show the radial profile of the median temperature of the 20 sparks (black solid lines) and the expected decrease of temperature up to the border of the plasma sheath (black dashed lines). Bluish shape represents the radial profile of the median brightness of the above-mentioned 20 spark, normalized to the maximum brightness of the median spectrum. Left axes of the inner panels show a zoom in the radial profile of the median brightness between 5 and 16 mm. Four different regions are discerned along the sparks radius: An inner core of 2 mm radius that includes regions I and II, wrapped by an outer sheath of up to 4 mm  $\pm$  0.58 mm radius (region III) and a dim glow region from 4 mm up to 16 mm (region IV).

(Sousa-Martins et al., 2016) nor slitless (An et al., 2019, 2021) spectroscopy studies. An et al. (2019, 2021) provide the estimation of the radial profiles of temperature and conductivity starting from  $\sim$ 1 cm from the center of the plasma channel, while the spatial distribution of electron temperature and conductivity in the inner core of the lightning remains unexplored. As for the physical interpretation of the temperature peak at the edge,

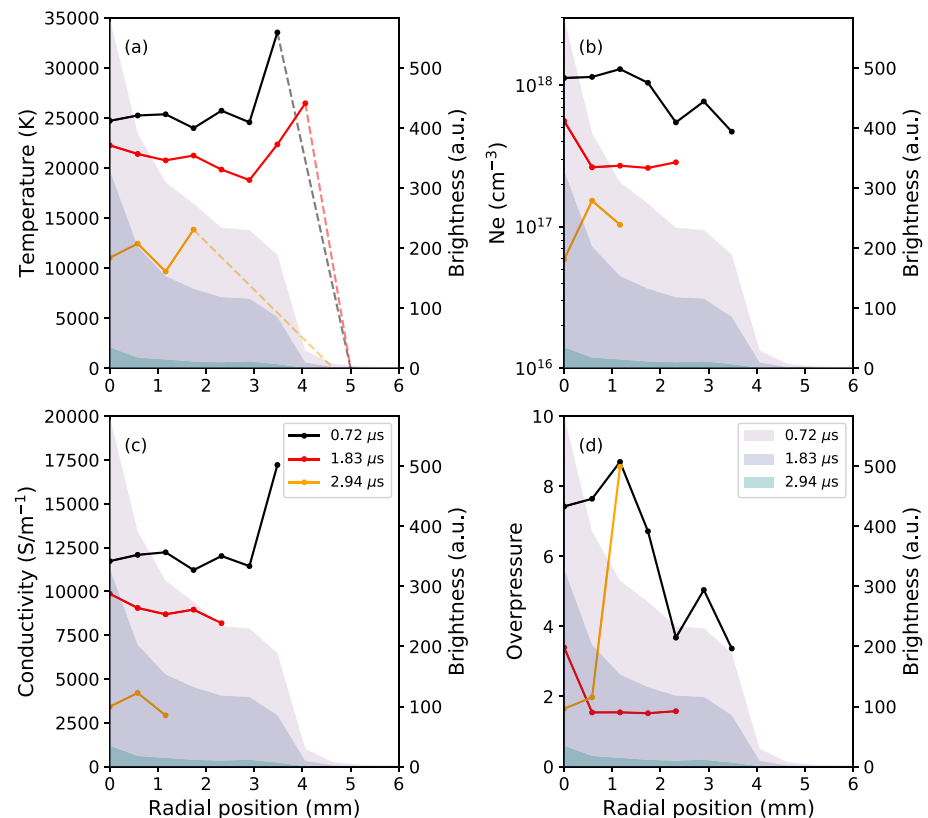


**Figure 8.** Radial profiles and their time evolution of (a) electron/gas temperature, (b) electron density, (c) electrical conductivity and (d) overpressure, in black, red, and yellow solid lines, for spark number 7. Right axes of all panels show the brightness level in arbitrary units. The evolution of the radial profile of the brightness is plotted in purple, blue and greenish shadowed areas. Dashed lines in panel (a) indicate the expected decrease of electron/gas temperature up to the border of the plasma sheath.

radiative shocks can exhibit high temperature spikes as earlier reported (Mihalas & Mihalas, 1984; Zel'Dovich & Raizer, 2002; Zinn & Anderson, 1973). According to Zinn and Anderson (1973) the peak temperature (or spike) at the front of the shock is associated with irreversible compression of the preheated air. This behavior is observed in Figure 5 (case of 5 μs) of Ripoll, Zinn, Jeffery, & Colestock (2014), and (b) in Figure 4 of Zinn and Anderson (1973).

From panel (b) of Figure 8, we infer that the radial profiles of the electron density in spark number 7 follow the radial profiles of brightness as time goes by. They show their maximum value in the inner core of the spark and decrease gradually along the radial dimension and time. This trend of the radial profiles of the electron density is also found in Sousa-Martins et al. (2016, 2019). This decreasing trend with time is also observed in lightning-like discharges (Kieu et al., 2020), although it is not found to be that steep in natural (Orville, 1968) and triggered lightning (Walker & Christian, 2019). We are not able to detect the electron density peak that should rise up in region IV as predicted in Figure 5 of Ripoll, Zinn, Jeffery, & Colestock (2014) and Figures 5 and 6 of Bocharov et al. (2021) due to the low SNR we have in that area.

The experimental values of the radial profiles of electron/gas temperature (10,000–34,000 K) and electron density ( $2 \times 10^{16} \text{ cm}^{-3} - 2 \times 10^{18} \text{ cm}^{-3}$ ) calculated in this study are very similar to those found in lightning-like discharges (Kieu et al., 2020), in natural return strokes (Orville, 1968) and in triggered lightning return strokes (Walker & Christian, 2019); the electrical conductivity values (2,500–17,500 S/m, see panel (c) of Figure 8) are also comparable to those found in natural return strokes (An et al., 2021) and in lightning-like discharges (Kieu et al., 2020; Sousa-Martins et al., 2016). Figure 8 panel (c) shows a peak of the electrical conductivity in region

III directly related to the electron (gas) temperature peak in that region. No peak in the radial profile of the electrical conductivity is found in the same region of the plasma channel in Figure 13 of Sousa-Martins et al. (2016).

Values in panel (d) of Figure 8 vary between  $\delta_p = 1$  (ambient pressure) and  $\delta_p = 9$ , which is comparable to those values found in lightning-like discharges (Kieu et al., 2020), and triggered lightning (Walker & Christian, 2019). We can see an enhancement of the overpressure in the border of the inner core of the lightning-like plasma channel, being this shape in agreement with the radial profile of the pressure in a lightning stroke of 60 J/cm, modeled in a previous research (Lacroix et al., 2019). Notice that the injected energy in the present work is 0.18 J/cm. One might think that this fact is the reason to find the same shape, but at different times. The same shape is also found in the radial profile of the electrical conductivity in Sousa-Martins et al. (2019) when they use the SuperDICOM lightning high-current generator at 100 kA.

Left axes of Figure 9 show the evolution of the radial profiles of the electron density and the populations of some chemical species ( $N_2$ , NO,  $O_2$ , OH,  $H_2$ ,  $N_2O$ ,  $NO_2$ ,  $HO_2$ ,  $O_3$ , and  $H_2O$ ) produced along the radius of the heated channel of a humid (50% relative humidity) air plasma and its variation with time for spark number 7, calculated from the peak pressure ( $\delta_p$ ) and assuming that they were produced under equilibrium conditions. The right axes of Figure 9 show the evolution of the radial profile of the electron/gas temperature (black dotted-dashed solid line) of spark number 7. Panel (a) corresponds to 0.72  $\mu s$  sampling time. In this first time stage the profiles follow a constant trend through the inner core up to  $\sim 3$  mm where the outer sheath region begins and the concentrations start to decrease as a possible reaction to the enhancement of the electron/gas temperature through the outer sheath of the plasma channel. Panel (b) of Figure 9 corresponds to 1.83  $\mu s$  sampling time. In this stage the radial profiles of the above-mentioned populations increase as electron temperature decreases, showing a small enhancement in the inner core region, where the electron density remains constant and the electron/gas temperature decrease, to finally decrease in the outer region, where the electron density decreases and the electron/gas temperature increases. Finally, panel (c) of Figure 9 corresponds to 2.94  $\mu s$  sampling time, and shows a significant increase of the above-mentioned concentrations when compared to the initial stages, due to the drastic decrease in the electron temperature for these radial positions at the final temporal stage of the lightning-like plasma discharge.

By looking at Figures 9 and 11 we can see that there are two groups of molecular species produced in the heated lightning channel. The first group is formed by (in decreasing order of importance)  $N_2$ , NO,  $O_2$ , OH, and  $H_2$ . The second group is made of  $N_2O$ ,  $NO_2$ ,  $HO_2$ ,  $O_3$ , and  $H_2O$ . At the early time stages (0.72  $\mu s$ , 1.83  $\mu s$ ) the two groups are clearly separated. However, the two groups become closer as time progresses (see panel (c) for 2.94  $\mu s$ ). In general, the concentration profiles of molecular species that we could estimate from  $\delta_p$  exhibit a flat radial shape except for the very early time at 0.72  $\mu s$ , decreasing in region III. Due to the low SNR, we are not able to estimate the concentrations of these molecular species in the hatched-shadowed area, where they are predicted to rise up and then decrease according to Figure 5 in Ripoll, Zinn, Jeffery, & Colestock (2014). Notice that concentrations in panel (c) of Figure 9 are higher than in panel (c) of Figure 11. This is due to the lower temperature measured in the last stage of spark 7 compared to the rest of sparks. Moreover, it is important to note that the trend shown by the concentrations of key species such as electrons, NO, OH and  $HO_2$  at the edge of the front (between 0.5 and 1 mm) at 2.94  $\mu s$  in Figure 9c is in reasonable agreement with the model predicted concentrations at 10  $\mu s$  shown in Figure 5 (top panel) of Ripoll, Zinn, Jeffery, & Colestock (2014). As in Figure 5 (top panel) of Ripoll, Zinn, Jeffery, & Colestock (2014), the electron density slightly decreases just before the edge while NO, OH and  $HO_2$  experimentally exhibit the start of a sharp rise that is not experimentally recorded (due to lack of SNR) though it is predicted by the model.

Recent airborne observations (Brune et al., 2021) and laboratory experimental results (Jenkins et al., 2021) confirm that considerable amounts of oxidant species (OH,  $HO_2$ ) could be directly produced by visible and subvisible (corona) electrical discharges in thunderstorms. Our results for the early time ( $< 4 \mu s$ ) dynamics of high temperature lightning-like discharges indicate that, at a constant pressure of  $\sim 940$  hPa and  $\sim 50\%$  relative humidity, direct production of OH in the heated channel is the second most important after that of nitrogen oxide (NO), but it is always considerable larger than that of  $HO_2$ . In contrast to this, experimental results (Jenkins et al., 2021) show slightly higher amounts of  $HO_2$  than of OH. However, as also pointed out by Jenkins et al. (2021), this could be due to the delayed measurements carried out 25 milliseconds after the flash. It could well be that at later times (from a few to tens of milliseconds) the cooling and accompanying non-equilibrium kinetics occurring in the lightning-like channel lead to similar, non-negligible (and probably measurable) concentrations of OH and  $HO_2$  at the edge of the lightning channel where the concentrations of NO and  $NO_2$  are very small as predicted by

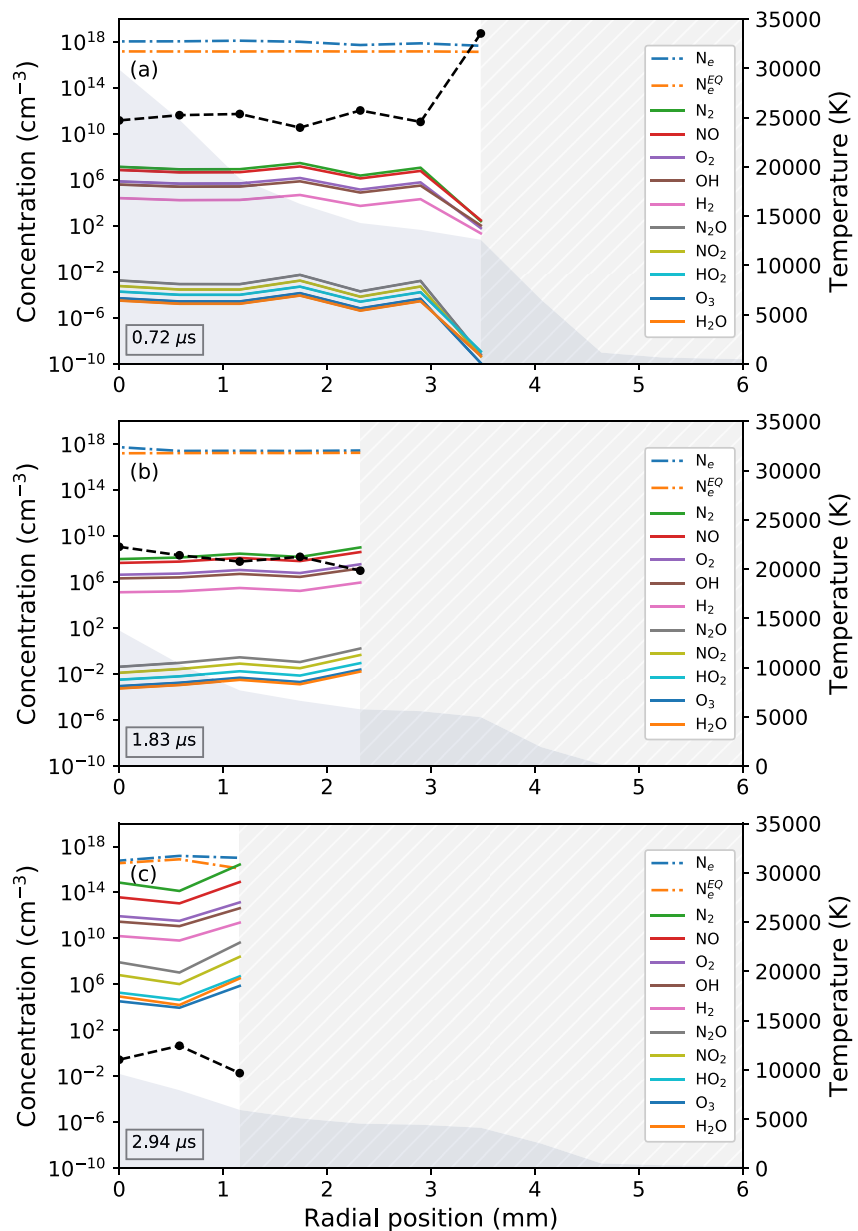


**Figure 9.** Radial profiles of measured (dashed blue) and equilibrium (dashed orange) electron density and populations of  $N_2$ ,  $NO$ ,  $O_2$ ,  $OH$ ,  $H_2$ ,  $N_2O$ ,  $NO_2$ ,  $HO_2$ ,  $O_3$ , and  $H_2O$ , at different sampling times, for spark number 7 (left axes, species in legend). Radial profiles of the electron/gas temperature at different sampling times, for spark number 7 (right axes, black dotted-dashed solid lines). Evolution of the radial profile of the normalized brightness (purple shadowed area, arbitrary units). Hatched areas with oblique lines cover the region where the signal-to-noise ratio (SNR) is so low that the measurements of electron density, electron/gas temperature and concentrations are not reliable.

1D (radial) time dependent models of the lightning channel for different input energies (Ripoll, Zinn, Jeffery, & Colestock, 2014).

The production of  $OH$  and  $HO_2$  recently reported by Jenkins et al. (2021) could also be due to air plasma streamers in corona discharges occurring in thunderstorm anvils since thundercloud coronas (Li et al., 2021; Soler et al., 2020) are now known to be more frequent (about 10 per second worldwide) (Soler et al., 2021) than previously suspected. Corona discharges in thunderclouds are especially frequent in the Tornado alley in North America (Soler et al., 2021) where the airborne observations (Brune et al., 2021) reporting important production of  $OH$  and  $HO_2$  were carried out. In addition, recent submillimeter-wave spectroscopy observations (Yamada

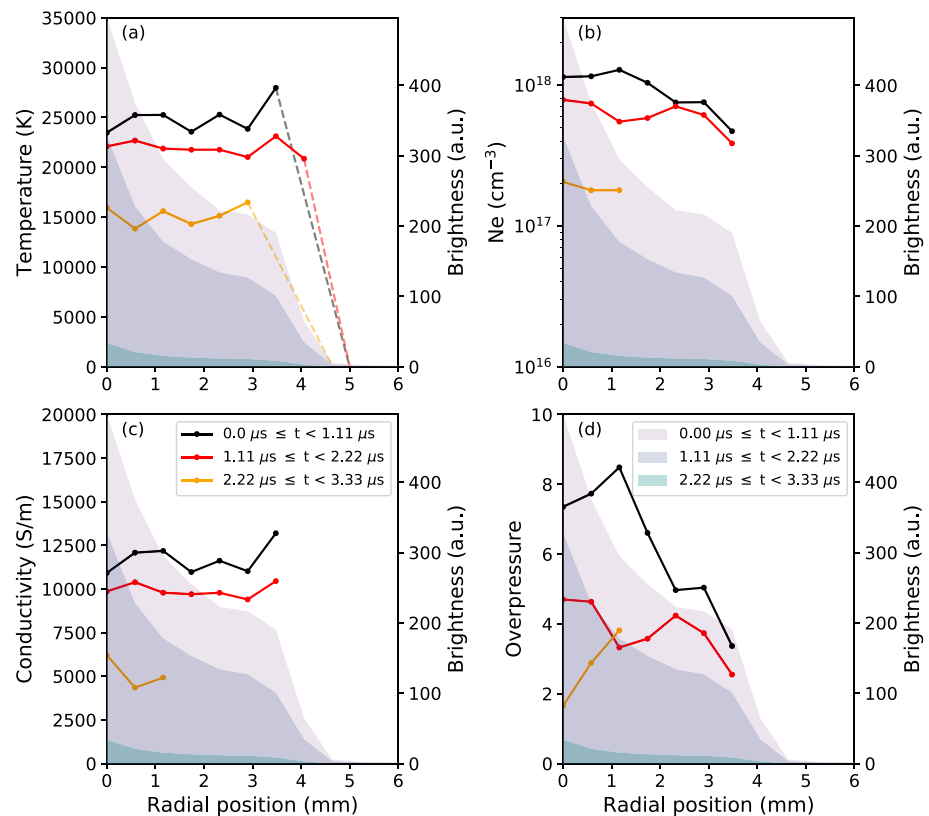


**Figure 10.** Radial profiles and their time evolution of (a) electron/gas temperature, (b) electron density, (c) electrical conductivity and (d) overpressure, in black, red and yellow solid lines, for the 20 recorded sparks. Right axes of all panels show the brightness level in arbitrary units. The evolution of the radial profile of the brightness is plotted in purple ( $0 \leq t < 1.11 \mu\text{s}$ ), blue ( $1.11 \leq t < 2.22 \mu\text{s}$ ), and greenish ( $2.22 \leq t < 3.33 \mu\text{s}$ ) shadowed areas, for the 20 recorded sparks. Dashed lines in panel (a) indicate the expected decrease of electron/gas temperature up to the border of the plasma sheath.

et al., 2020) indicate that streamer coronas in sprites (Gordillo-Vázquez, 2008; Gordillo-Vázquez et al., 2018; Sentman et al., 2008) occurring in the mesosphere are responsible of mesospheric OH and HO<sub>2</sub> enhancements. Previous observations (Bozem et al., 2014; Zahn et al., 2002) relate sudden O<sub>3</sub> enhancements found in thunderstorms with the occurrence of subvisible (corona) discharges in thunderclouds. It is therefore quite possible that the significant OH and HO<sub>2</sub> enhancements recently found in electrified anvil clouds (Brune et al., 2021) are due to the non-equilibrium kinetics (Gordillo-Vázquez & Donkó, 2009) driven by streamers in corona discharges (Simek et al., 2002). Our measurements and estimations in the present work indicate that, as expected, O<sub>3</sub> is specially depressed by the high temperatures in the heated channel.

Finally, it is worth highlighting that the trends observed in Figures 8 and 9 for one spark are also observed in the 20 recorded sparks, as Figures 10 and 11 show. To generate Figure 10 we aligned the 2D spatial-spectral images of the 20 sparks with respect to their inner core grouping them according to the sampling time of the sparks, that is, below 1.11 μs, between 1.11 and 2.22 μs, and after 2.22 μs, so that we could calculate the median values of the radial profiles of the electron/gas temperature (Figure 10a), electron density (Figure 10b), electrical conductivity (Figure 10c) and overpressure (Figure 10d). We only considered valid median values at a certain radial position when there were more than 5 sparks with a valid value of electron/gas temperature or electron density for that radial position. As Figure 10 shows similar trends than Figure 8, we can conclude that the previous discussion is valid for most sparks. The median radial profiles of the concentration of the above-mentioned species follow the same trend as well if we compare Figures 9 and 11, but in this case we reach further radial positions that suggest that these radial profiles somehow follow the shape of the brightness of the spark, excepting the latter time stages of the sparks, when the concentrations seem to increase as we move away from the core of the spark.

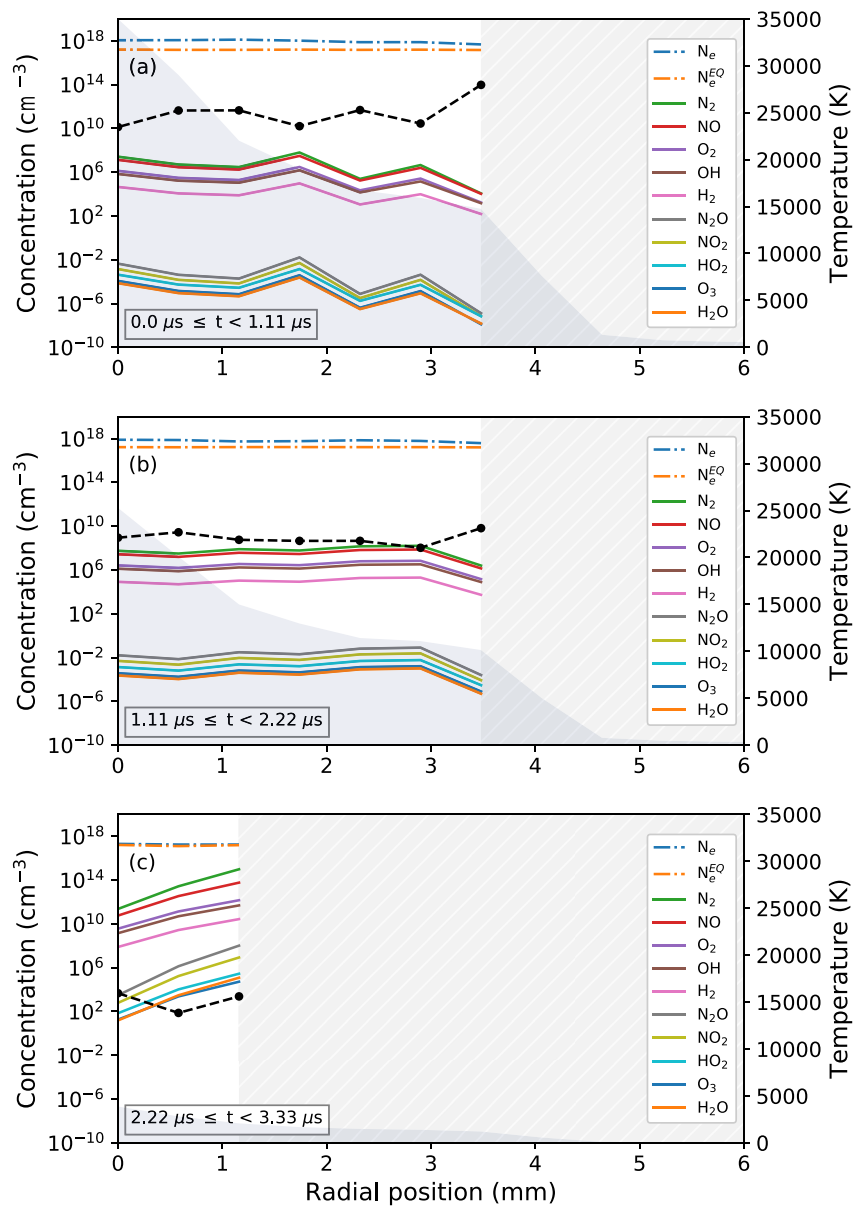


**Figure 11.** Radial profiles of the median value of the measured (dashed blue) and equilibrium (dashed orange) electron density and populations of  $N_2$ ,  $NO$ ,  $O_2$ ,  $OH$ ,  $H_2$ ,  $N_2O$ ,  $NO_2$ ,  $HO_2$ ,  $O_3$ , and  $H_2O$ , at different sampling times, from the 20 recorded sparks (left axes, species in legend). Median value of the radial profiles of the electron/gas temperature at different sampling times, from the 20 recorded sparks (right axes, black dotted-dashed solid lines). Evolution of the median radial profile of the normalized brightness, from the 20 recorded sparks (purple shaded area, arbitrary units). Hatched areas with oblique lines cover the region where the signal-to-noise ratio (SNR) is so low that the measurements of electron density, electron/gas temperature and concentrations are not reliable.

Studying the submicrosecond/microsecond time dynamics of small (a few centimeter long) lightning-like (arc) discharges produced with small peak current impulses (of several hundred Amperes) allow to reproduce the trends and values of the electron density and gas temperature found in natural (Boggs et al., 2021; Orville, 1968) and/or triggered lightning strokes (Walker & Christian, 2019). Because the current (of several hundreds amperes) and voltage (several tens of thousand volts) used are low, so is the input electrical energy (which is much lower than in real lightning strokes). Still, the behavior (and the radial absolute values) of the concentrations of chemical components during the early stages of the heated stroke channel can be reasonably reproduced experimentally as we have seen by comparing with recent models for the expansion dynamics of lightning strokes (Ripoll, Zinn, Jeffery, & Colestock, 2014; Ripoll, Zinn, Colestock, & Jeffery, 2014). However, a small discharge cannot



reproduce the real spatial (radial) dimensions of an expanding lightning stroke channel. In spite of this, we can still consider small arcs as good analogs of real and/or triggered lightning but with the advantage of having an easier access to them in the laboratory. The challenge ahead is to study the late temporal stages that, because of the lower luminosity, complicates their optical diagnostics. The effort, however, could be worth because, according to modeling (Ripoll, Zinn, Jeffery, & Colestock, 2014), the largest chemical production of  $\text{NO}_x$ , OH, and  $\text{HO}_2$  in lightning strokes occurs during the cooling phase at lower gas temperatures (below 10,000 K).

## 5. Summary and Conclusions

In this work we analyzed the radial profiles of the spectral brightness of 20 lightning-like plasma discharges from experimental spectroscopic data recorded at 900 kfps and 0.79  $\mu\text{s}$  exposure time. This is the first direct measurement of the radial profiles of gas temperature, electron density, pressure and conductivity in lightning-like plasma channels. Previous works estimate these radial profiles from 1D (only spectral, no spatial) spectroscopy combined with the radiative transfer equation and modeling. This is the first time that these radial profiles are measured directly from 2D (spatial-spectral) images, without losing the spatial dimension of the spectra. Here we propose a method able to confirm the reliability of such 2D theoretical modeling.

We found that the optical emissions of the sparks are initially ( $<1.11 \mu\text{s}$ ) dominated by the  $\text{N}_2$  first positive system at 660.8 nm, while the N II ion line at 661.05 nm is very significant below 4 mm. N II ions at 648.20 and 661.05 nm start to prevail over the rest of emissions within the outer dim glow region (10–14 mm). A damped oscillating behavior along the radius of the spark is detected for all emissions, with a variable period. After 1.11  $\mu\text{s}$  and before 2.22  $\mu\text{s}$  we find that  $\text{H}_\alpha$  and O II (656.54 nm) spectral lines dominate clearly over the rest of emissions until 9 mm, where N II ion line at 648.20 nm rises up. After 2.22  $\mu\text{s}$ ,  $\text{H}_\alpha$  and O II (656.54 nm) spectral lines dominate also below 4 mm, and no spectral signatures are found beyond.

From these measurements we found that the electron/gas temperature remains almost constant along the inner core of the spark whereas it increases in the external border of the spark sheath before 2.22  $\mu\text{s}$ . This trend is consistent with the results obtained from 1D cylindrical radiation-hydrodynamic simulations using an exact (the discrete-ordinates method (DOM-S12)) and approximate (the P1 model approach) solutions of the radiation transfer equations (Ripoll, Zinn, Jeffery, & Colestock, 2014). We also found a decrease of the electron/gas temperature in the inner core (up to  $\sim 2$  mm) of the spark as time progresses. The electrical conductivity also follows this behavior. We found that the calculated trend of the radial profile of the electron density follows the shape of the radial profile of the brightness of the spark. This translates into an enhancement of the overpressure in the border of the inner core of the lightning-like plasma channel at the first (0.72  $\mu\text{s}$ ) and third time (2.94  $\mu\text{s}$ ) stages of the plasma discharge.

Finally, we also estimated the evolution of the radial profile of the populations of NO,  $\text{O}_2$ , OH,  $\text{H}_2$ ,  $\text{N}_2\text{O}$ ,  $\text{NO}_2$ ,  $\text{HO}_2$ ,  $\text{O}_3$ , and  $\text{H}_2\text{O}$  produced along the radius of the lightning-like plasma channels from the peak pressure  $\delta_p$  and assuming that they were produced from humid (50%) air under equilibrium conditions. At initial time stages (0.72  $\mu\text{s}$ ), the radial profiles of the above-mentioned populations follow a constant trend up to the inner core (up to  $\sim 2$  mm), where the populations start to slightly decrease. Afterward, they show a small enhancement (up to  $\sim 3$  mm) in between the inner and outer sheath regions to finally decrease in the outer region. We also found a huge increase (compared to the initial time stages) of the chemical species concentrations in the inner core of the plasma channel following the gas temperature decrease. Hydroxyl (OH) is found to be the second most abundant molecular species (only after nitrogen oxide (NO)) directly generated by heated lightning-like channels, while ozone is the least directly produced.

## Data Availability Statement

Data sets for this research and related software for figure generation are available through GitHub (Passas-Varo et al., 2022), under GNU General Public License. Figures were made with Matplotlib version 3.5.1 (Hunter, 2007), available under the Matplotlib license at <https://matplotlib.org/>.

### Acknowledgments

This work has received funding from the European Union Horizon 2020 research and innovation program under the Marie Skłodowska-Curie grant agreement SAINT 722337. Additionally, this work was supported by the Spanish Ministry of Science and Innovation, MINECO, under project PID2019-109269RB-C43 and FEDER program. M. Passas-Varo, F. J. Gordillo-Vázquez, J. Sánchez, and N. Kieu acknowledge financial support from the State Agency for Research of the Spanish MCIU through the Center of Excellence Severo Ochoa's award for the Instituto de Astrofísica de Andalucía (SEV-2017-0709).

### References

- An, T., Yuan, P., Liu, G., Cen, J., Wang, X., Zhang, M., & An, Y. (2019). The radius and temperature distribution along radial direction of lightning plasma channel. *Physics of Plasmas*, 26(1), 013506. <https://doi.org/10.1063/1.5059363>
- An, T., Yuan, P., Wan, R., Chen, R., Liu, G., Cen, J., & Wang, X. (2021). Conductivity characteristics and corona sheath radius of lightning return stroke channel. *Atmospheric Research*, 258, 105649. <https://doi.org/10.1016/j.atmosres.2021.105649>
- Arns, J. A., Colburn, W. S., & Barden, S. C. (1999). Volume phase gratings for spectroscopy, ultrafast laser compressors, and wavelength division multiplexing. *Current developments in optical design and optical engineering viii*, 3779, 313–323.
- Bocharov, A., Mareev, E., & Popov, N. (2021). Numerical simulation of high-current pulsed arc discharge in air. *Journal of Physics D: Applied Physics*, 55(11), 115204. <https://doi.org/10.1088/1361-6463/ac3866>
- Boggs, L. D., Liu, N., Nag, A., Walker, T. D., Christian, H. J., da Silva, C. L., et al. (2021). Vertical temperature profile of natural lightning return strokes derived from optical spectra. *Journal of Geophysical Research: Atmospheres*, 126(8), e2020JD034438. <https://doi.org/10.1029/2020jd034438>
- Bozem, H., Fischer, H., Gurk, C., Schiller, C., Parchatka, U., Koenigstedt, R., et al. (2014). Influence of corona discharge on the ozone budget in the tropical free troposphere: A case study of deep convection during Gabriel. *Atmospheric Chemistry and Physics*, 14(17), 8917–8931. <https://doi.org/10.5194/acp-14-8917-2014>
- Brune, W., McFarland, P., Bruning, E., Waugh, S., MacGorman, D., Miller, D., et al. (2021). Extreme oxidant amounts produced by lightning in storm clouds. *Science*, 372(6543), 711–715. <https://doi.org/10.1126/science.abg0492>
- Carbone, E., D'Isa, F., Hecimovic, A., & Fantz, U. (2020). Analysis of the C2 swan bands as a thermometric probe in CO<sub>2</sub> microwave plasmas. *Plasma Sources Science and Technology*, 29(5), 055003. <https://doi.org/10.1088/1361-6595/ab74b4>
- Cen, J., Yang, C., Yang, S., Li, Z., & Zhang, J. (2022). A spectral comparison of lightning discharge plasma and laser-induced air plasma. *AIP Advances*, 12(6), 065202. <https://doi.org/10.1063/5.0093322>
- Dufay, M. (1926). Spectres des éclairs. *Comptes Rendus*, 182, 1331–1333.
- Fantz, U. (2006). Basics of plasma spectroscopy. *Plasma Sources Science and Technology*, 15(4), S137–S147. <https://doi.org/10.1088/0963-0252/15/4/s01>
- Gigosos, M. A., González, M. A., & Cardenoso, V. (2003). Computer simulated balmer-alpha, -beta and -gamma Stark line profiles for non-equilibrium plasmas diagnostics. *Spectrochimica Acta Part B: Atomic Spectroscopy*, 58(8), 1489–1504. (5th European Furnace Symposium and 10th International Solid Sampling Colloquium with Atomic Spectroscopy). [https://doi.org/10.1016/S0584-8547\(03\)00097-1](https://doi.org/10.1016/S0584-8547(03)00097-1)
- Godin, D., & Trépanier, J. (2004). A robust and efficient method for the computation of equilibrium composition in gaseous mixtures. *Plasma Chemistry and Plasma Processing*, 24(3), 447–473. <https://doi.org/10.1007/s11090-004-2279-8>
- Gordillo-Vázquez, F. J. (2008). Air plasma kinetics under the influence of sprites. *Journal of Physics D*, 41(23), 234016. <https://doi.org/10.1088/0022-3727/41/23/234016>
- Gordillo-Vázquez, F. J., & Donkó, Z. (2009). Electron energy distribution functions and transport coefficients relevant for air plasmas in the troposphere: Impact of humidity and gas temperature. *Plasma Sources Science and Technology*, 18(3), 034021. <https://doi.org/10.1088/0963-0252/18/3/034021>
- Gordillo-Vázquez, F. J., Passas, M., Luque, A., Sánchez, J., Van der Velde, O. A., & Montanyá, J. (2018). High spectral resolution spectroscopy of sprites: A natural probe of the mesosphere. *Journal of Geophysical Research: Atmospheres*, 123(4), 2336–2346. <https://doi.org/10.1002/2017jd028126>
- Hill, G. J., Wolf, M. J., Tufts, J. R., & Smith, E. C. (2003). Volume phase holographic (vph) gratings for optical and infrared spectrographs. In *Specialized optical developments in astronomy* (Vol. 4842(1–9)).
- Hunter, J. D. (2007). Matplotlib: A 2D graphics environment. *Computing in Science & Engineering*, 9(3), 90–95. <https://doi.org/10.1109/MCSE.2007.55>
- Jenkins, J. M., Brune, W. H., & Miller, D. O. (2021). Electrical discharges produce prodigious amounts of hydroxyl and hydroperoxyl radicals. *Journal of Geophysical Research: Atmospheres*, 126(9), e2021JD034557. <https://doi.org/10.1029/2021jd034557>
- Kieu, N., Gordillo-Vázquez, F. J., Passas, M., Sánchez, J., & Pérez-Invernón, F. J. (2021). High-speed spectroscopy of lightning-like discharges: Evidence of molecular optical emissions. *Journal of Geophysical Research: Atmospheres*, 126(11), e2021JD035016. <https://doi.org/10.1029/2021jd035016>
- Kieu, N., Gordillo-Vázquez, F. J., Passas-Varo, M., Sánchez, J., Pérez-Invernón, F. J., Luque, A., et al. (2020). Submicrosecond spectroscopy of lightning-like discharges: Exploring new time regimes. *Geophysical Research Letters*, 47(15), e2020GL088755. <https://doi.org/10.1029/2020GL088755>
- Kramida, A., Ralchenko, Y., & Reader, J. (2020). *NIST atomic spectra database*. National Institute of Standards and Technology. (version 5.8), [Online]. Retrieved from <https://physics.nist.gov/asd>
- Lacroix, A., Coulouvat, F., Marchiano, R., Farges, T., & Ripoll, J.-f. (2019). Acoustical energy of return strokes: A comparison between a statistical model and measurements. *Geophysical Research Letters*, 46(20), 11479–11489. <https://doi.org/10.1029/2019gl085369>
- Li, D., Luque, A., Gordillo-Vázquez, F. J., Liu, F., Lu, G., Neubert, T., et al. (2021). Blue flashes as counterparts to narrow bipolar events: The optical signal of shallow in-cloud discharges. *Journal of Geophysical Research: Atmospheres*, 126(13), e2021JD035013. <https://doi.org/10.1029/2021jd035013>
- Mihalas, D., & Mihalas, B. (1984). *Foundations of radiation hydrodynamics*. Oxford University Press.
- Orville, R. E. (1968). A high-speed time-resolved spectroscopic study of the lightning return stroke: Part ii. a quantitative analysis. *Journal of the Atmospheric Sciences*, 25(5), 839–851. [https://doi.org/10.1175/1520-0469\(1968\)025<0839:ahstrs>2.0.co;2](https://doi.org/10.1175/1520-0469(1968)025<0839:ahstrs>2.0.co;2)
- Parra-Rojas, F. C., Passas, M., Carrasco, E., Luque, A., Tanarro, I., Simek, M., & Gordillo-Vázquez, F. J. (2013). Spectroscopic diagnostics of laboratory air plasmas as a benchmark for spectral rotational (gas) temperature determination in tles. *Journal of Geophysical Research: Space Physics*, 118(7), 4649–4661. <https://doi.org/10.1002/jgra.50433>
- Passas, M., Madiedo, J. M., & Gordillo-Vázquez, F. J. (2016). High resolution spectroscopy of an orionid meteor from 700 to 800 nm. *Icarus*, 266, 134–141. <https://doi.org/10.1016/j.icarus.2015.11.020>
- Passas, M., Sánchez, J., Sánchez-Blanco, E., Luque, A., & Gordillo-Vázquez, F. J. (2016). Grassp: A spectrograph for the study of transient luminous events. *Applied Optics*, 55(23), 6436–6442. <https://doi.org/10.1364/ao.55.006436>
- Passas-Varo, M., Sánchez, J., & Gordillo-Vázquez, F. J. (2022). Dataset and software to generate figures for jgr: “Atmospheres experimental radial profiles of early time neutral and ion spectroscopic signatures in lightning-like discharges”. [Dataset]. Zenodo. <https://doi.org/10.5281/zenodo.6473251>
- Passas-Varo, M., Sánchez, J., Kieu, T. N., Sánchez-Blanco, E., & Gordillo-Vázquez, F. J. (2019). Galius: An ultrafast imaging spectrograph for the study of lightning. *Applied Optics*, 58(29), 8002–8006. <https://doi.org/10.1364/AO.58.008002>

- Prueitt, M. L. (1963). The excitation temperature of lightning. *Journal of Geophysical Research*, 68(3), 803–811. <https://doi.org/10.1029/JZ068i003p00803>
- Raizer, Y. P., & Allen, J. E. (1991). *Gas discharge physics* (Vol. 1). Springer.
- Ripoll, J. F., Zinn, J., Colestock, P. L., & Jeffery, C. A. (2014). On the dynamics of hot air plasmas related to lightning discharges: 2. Electrodynamic. *Journal of Geophysical Research: Atmospheres*, 119(15), 9218–9235. <https://doi.org/10.1002/2013jd020068>
- Ripoll, J. F., Zinn, J., Jeffery, C. A., & Colestock, P. L. (2014). On the dynamics of hot air plasmas related to lightning discharges: 1. Gas dynamics. *Journal of Geophysical Research: Atmospheres*, 119(15), 9196–9217. <https://doi.org/10.1002/2013jd020067>
- Robledo-Martinez, A., Sobral, H., & Ruiz-Meza, A. (2008). Time-resolved diagnostic of an impulse discharge in variable pressure air. *Journal of Physics D*, 41(17), 175207. <https://doi.org/10.1088/0022-3727/41/17/175207>
- Sentman, D., Stenbaek-Nielsen, H., McHarg, M., & Morrill, J. (2008). Plasma chemistry of sprite streamers. *Journal of Geophysical Research*, 113(D11), D11112. <https://doi.org/10.1029/2007jd008941>
- Simek, M., DeBenedictis, S., Dilecce, G., Babický, V., Clupek, M., & Sunka, P. (2002). Time and space resolved analysis of N<sub>2</sub>(C<sup>3</sup>Π<sub>g</sub>) vibrational distributions in pulsed positive corona discharge. *Journal of Physics D*, 35(16), 1981–1990. <https://doi.org/10.1088/0022-3727/35/16/312>
- Slipher, V. M. (1917). The spectrum of lightning. *Lowell Observatory Bulletin*, 3, 55–58.
- Soler, S., Gordillo-Vázquez, F. J., Pérez-Invernón, F. J., Luque, A., Li, D., Neubert, T., et al. (2021). Global frequency and geographical distribution of nighttime streamer corona discharges (blues) in thunderclouds. *Geophysical Research Letters*, 48(18), e2021GL094657. <https://doi.org/10.1029/2021gl094657>
- Soler, S., Pérez-Invernón, F. J., Gordillo-Vázquez, F. J., Luque, A., Li, D., Malagón-Romero, A., et al. (2020). Blue optical observations of narrow bipolar events by ASIM suggest corona streamer activity in thunderstorms. *Journal of Geophysical Research: Atmospheres*, 125(16), e2020JD032708. <https://doi.org/10.1029/2020jd032708>
- Sousa-Martins, R., Zaepffel, C., Chemartin, L., Lalande, P., & Lago, F. (2019). Characterization of high-current pulsed arcs ranging from 100–250 ka peak. *Journal of Physics D: Applied Physics*, 52(18), 185203. <https://doi.org/10.1088/1361-6463/ab0190>
- Sousa-Martins, R., Zaepffel, C., Chemartin, L., Lalande, P., & Soufiani, A. (2016). Characterization of a high current pulsed arc using optical emission spectroscopy. *Journal of Physics D: Applied Physics*, 49(41), 415205. <https://doi.org/10.1088/0022-3727/49/41/415205>
- Thomsen, V., Schatzlein, D., & Mercuro, D. (2003). Limits of detection in spectroscopy. *Spectroscopy*, 18(12), 112–114.
- Uman, M. (1963). The continuum spectrum of lightning. *Journal of Atmospheric and Terrestrial Physics*, 25(5), 287–295. [https://doi.org/10.1016/0021-9169\(63\)90025-4](https://doi.org/10.1016/0021-9169(63)90025-4)
- Walker, T. D., & Christian, H. J. (2017). Triggered lightning spectroscopy: Part 1. A qualitative analysis. *Journal of Geophysical Research: Atmospheres*, 122(15), 8000–8011. <https://doi.org/10.1002/2016jd026419>
- Walker, T. D., & Christian, H. J. (2019). Triggered lightning spectroscopy: Part 2. A quantitative analysis. *Journal of Geophysical Research: Atmospheres*, 124(7), 3930–3942. <https://doi.org/10.1029/2018jd029901>
- Weidman, C., Boye, A., & Crowell, L. (1989). Lightning spectra in the 850- to 1400-nm near-infrared region. *Journal of Geophysical Research*, 94(D11), 13249–13257. <https://doi.org/10.1029/jd094id11p13249>
- Yamada, T., Sato, T., Adachi, T., Winkler, H., Kuribayashi, K., Larsson, R., et al. (2020). HO<sub>2</sub> generation above sprite-producing thunderstorms derived from low-noise SMILES observation spectra. *Geophysical Research Letters*, 47(3), e60090. <https://doi.org/10.1029/2019GL085529>
- Zahn, A., Brenninkmeijer, C., Crutzen, P., Parrish, D., Sueper, D., Heinrich, G., & Heintzenberg, J. (2002). Electrical discharge source for tropospheric “ozone-rich transients”. *Journal of Geophysical Research*, 107(D22), 4638. ACH–16. <https://doi.org/10.1029/2002jd002345>
- Zel'Dovich, Y. B., & Raizer, Y. P. (2002). *Physics of shock waves and high-temperature hydrodynamic phenomena*. Courier Corporation.
- Zinn, J., & Anderson, R. (1973). Structure and luminosity of strong shock waves in air. *The Physics of Fluids*, 16(10), 1639–1644. <https://doi.org/10.1063/1.1694190>